ACS Medicinal Chemistry Letters

pubs.acs.org/acsmedchemlett Letter

Resorufin Enters the Photodynamic Therapy Arena: A Monoamine Oxidase Activatable Agent for Selective Cytotoxicity

Toghrul Almammadov, Gizem Atakan, Ozen Leylek, Gulnihal Ozcan,* Gorkem Gunbas,* and Safacan Kolemen*

Cite This: ACS Med. Chem. Lett. 2020, 11, 2491−2496 Read Online

ACCESS | Metrics & More | Article Recommendations | Supporting Information

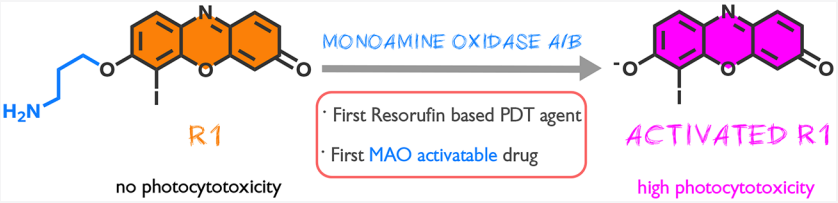

ABSTRACT: A red-absorbing, water-soluble, and iodinated resorufin derivative (**R1**) that can be selectively activated with a monoamine oxidase (MAO) enzyme was synthesized, and its potential as a photodynamic therapy (PDT) agent was evaluated. **R1** showed high $^1O_2$ generation yields in aqueous solutions upon addition of MAO isoforms, and it was further tested in cell culture studies. **R1** induced photocytotoxicity after being triggered by endogenous MAO enzyme in cancer cells with a much higher efficiency in SH-SY5Y neuroblastoma cells with high MAO-A expression. Additionally, **R1** displayed differential cytotoxicity between cancer and normal cells, without any considerable dark toxicity. To the best of our knowledge, **R1** marks the first example of a resorufin-based photosensitizer (PS) as well as the first anticancer drug that is activated by a MAO enzyme. Remarkably, the target PDT agent was obtained only in three steps as a result of versatile resorufin chemistry.

KEYWORDS: *Photodynamic therapy, activatable photosensitizers, resorufin, cancer cell selectivity, monoamine oxidase*

Photodynamic therapy (PDT) is a clinically approved treatment modality, which utilizes singlet oxygen ($^1O_2$) as a primary cytotoxic agent to kill the cells of interest.[1−4] PDT has been recognized as a promising alternative to conventional therapies as it offers minimally invasive procedures, opportunities for repeated application, negligible drug resistance, and immune system activation against tumors.[1] In a typical PDT action, generation of singlet oxygen is satisfied by combining three key components: light, a photosensitizer (PS), and molecular oxygen ($^3O_2$).[4] Despite its high therapeutic potential and clear advantages, broader acceptance of PDT in clinical practices is mainly restricted due to the limited penetration of the light through tissues and lack of cancer cell selectivity.[5] Although PDT has inherent selectivity to some extent, which arises from the fact that the excitation light can be precisely delivered to the tumor region, this mode of selectivity is not sufficient to eliminate undesired photodamage on skin and eyes as well as on other healthy cells.[5,6] Accordingly, conventional PDT drugs leave patients photosensitive up to months, forcing them to stay away from sunlight and in some cases even indoor light to avoid healthy cell death and severe post-treatment pain.[6] Among strategies to improve selectivity, activatable PSs have recently gained significant interest in the design of new generation PDT agents.[5,7] A similar approach is also widely used to design selective fluorophores for activity-based sensing applications.[8] In an activatable PDT approach, a cage group is covalently attached to PS and when the cage is cleaved, the PS goes from an OFF state to an ON state as a result of remarkable changes in their photophysical properties.[5,7] The $^1O_2$ generation occurs only when a PS at an ON state is illuminated. In general, caged groups are cleaved by tumor-associated stimuli that are differentially expressed by cancer cells, or better yet-specific to the type of cancer, and so the cleavage happens at the tumor site while sparing healthy tissue.[9−11] In the literature, the most widely used strategy is to employ biothiols[9] and hydrogen peroxide[10] as cancer related stimuli to accomplish the activation of PSs. Additionally, there are plenty of acidic pH activatable PSs[11] that take advantage of the acidic microenvironment to control the photocytotoxicity. Enzymes that are overexpressed in tumors have also attracted considerable attention in the design of activatable PSs especially after the role of certain enzymes in tumorigenesis became clear over the years.[5,7,12] Nevertheless, the majority of activatable PSs in the literature are based on first-generation

Received: September 4, 2020
Accepted: November 19, 2020
Published: November 23, 2020

https://dx.doi.org/10.1021/acsmedchemlett.0c00484
ACS Med. Chem. Lett. 2020, 11, 2491−2496

porphyrin and phthalocyanine skeletons,[5,13] which tend to form aggregates in aqueous medium due to their hydrophobic nature or several other PSs that absorb at shorter wavelengths with limited tissue penetration depth. In this context, great effort has been put forth to design red-shifted, water-soluble, and activatable PS cores in recent years.[14−17] However, PSs that show apparent differential cytotoxicity between cancer and healthy cells still remain elusive.

Resorufin is a long-known and highly attractive fluorescent probe due to its favorable properties such as water solubility, red-shifted absorption/emission signals, high fluorescence quantum yield, and absorption coefficient.[18] Furthermore, it is well-established that 7-hydroxy substitution on a resorufin core shifts the absorption maximum to shorter wavelengths and effectively quenches the fluorescence, which allows the design of activatable imaging probes.[18−20] In principle, the resorufin core can be easily adapted into PDT studies if an intersystem crossing (ISC) pathway, a required transition for $^1O_2$ generation, can be satisfied.

Monoamine oxidase (MAO) is a flavin-dependent oxidoreductase that catalyzes the oxidative deamination of amines to aldehydes and has two isoforms: MAO-A and MAO-B.[21] Recent studies have shown that MAO is overexpressed in several cancer cells, which is associated with tumor progression and metastasis as high MAO activity causes redox imbalance and triggers oxidative stress.[22−25] However, it has not yet been utilized in the scope of any therapeutic approach. Here, we report for the first time the conversion of fluorescent resorufin to an effective PS, which can be activated by a MAO enzyme selectively in cancer cells.

In the design of our PS **R1**, iodine was incorporated on to the core structure in order to facilitate heavy atom-mediated ISC. The core was also decorated with a propylamine cage group, which is known to be selectively removed by MAO isoforms,[19,26] to block the $^1O_2$ generation even under illumination (Figure 1). MAO-induced selective oxidation of

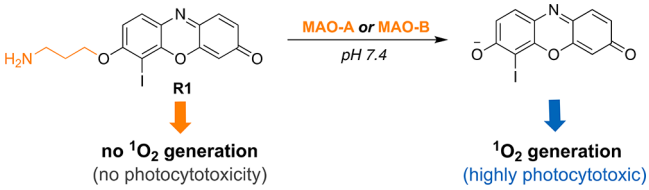

Figure 1. Molecular structure of **R1** and its activation with MAO isoforms.

amine and following β-elimination are expected to remove the cage group and consequently generate the corresponding active drug only in targeted cancer cells (Figure S1), where MAO expression is high, while sparing the noncancerous cells with low MAO activity.[27,28]

In the synthesis of **R1** (Figure 2), initially commercially available resorufin was reacted with Boc-protected 3-bromopropyl amine in the presence of Cs_2CO_3 to give compound **1**. Iodination was performed under the influence of iodine and iodic acid to yield iodo-resorufin derivative **2**. Unlike fluorescein derivatives, the iodination required much stronger conditions and resulted in only monoiodination compared to tetra-halogenations, which are quite common in the fluorescein core.[29] Standard Boc deprotection utilizing TFA was achieved in high yield to give the target compound

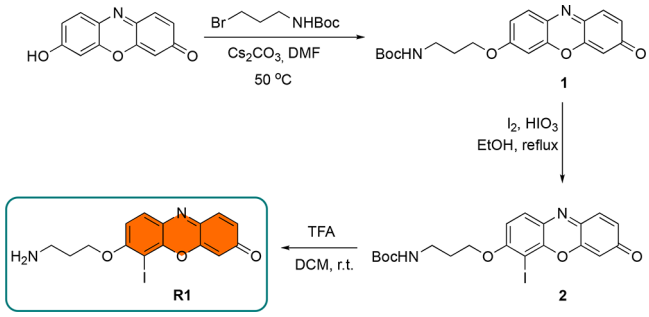

Figure 2. Synthetic pathway for **R1**.

R1. The synthesis was completed in three steps with 34% overall yield.

After completing the synthesis, we first investigated the photophysical properties of **R1** and its response to MAO isoforms (Figure 3a). **R1** exhibited a blue-shifted absorption

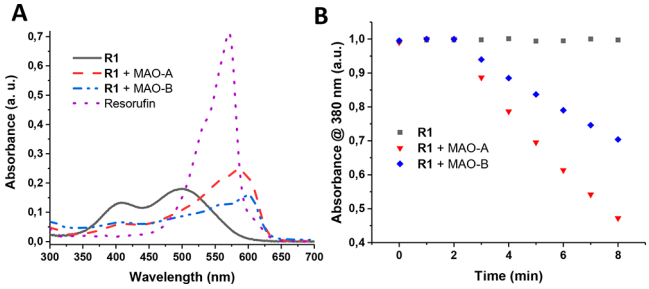

Figure 3. (a) Absorption spectra of **R1** (10 μM) before and after addition of MAO-A/B (20 μg/mL) and resorufin (10 μM) in PBS (1% DMSO, pH 7.4). (b) Relative $^1O_2$ generation efficiency of **R1** (10 μM) before and after addition of MAO-A/B (20 μg/mL) in PBS buffer (pH 7.4, 1% DMSO). During the first 2 min, the samples were kept in the dark.

maximum centered at 500 nm with a shoulder at 408 nm in aqueous solutions as a result of *O*-alkylation. Upon reacting with MAO-A/B for 3 h, absorption maxima were red-shifted (*ca.* 100 nm) and new peaks appeared at 588 and 595 nm respectively with a stronger signal in the case of MAO-A. Noticeable red-shift (*ca.* 25 nm) was observed compared to nonhalogenated parent resorufin core (Figure 3a, Table S1). **R1** is almost nonfluorescent in aqueous solutions before addition of the enzyme (Figure S2). After treating **R1** with MAO-A/B, very small increase in emission signals at 620 nm were detected over 3 h as a result of effective ISC (Figure S2, Table S1). Photostability of **R1** was confirmed by monitoring the absorption signal at 500 and 408 nm under continuous light (595 nm, 20 mW/cm^2) irradiation (Figure S3). Lipophilicity value (LogP) is another vital parameter for any drug candidate in perspective of molecular biology and pharmacology. In this direction, the LogP value of **R1** was calculated and found to be 0.412 ± 0.020, which is very similar to the parent resorufin core (0.427 ± 0.036).[30] It is a very well-known fact that MAO produces hydrogen peroxide (H_2O_2) as a catalytic byproduct.[24] Absorption spectra of H_2O_2 treated **R1** showed no change, clearly indicating that H_2O_2 is not reacting with **R1** (Figure S4).

The $^1O_2$ generation capacity of **R1** was initially evaluated chemically by using a water-soluble anthracene-based trap molecule 2,2′-(anthracene-9,10-diyl)bis(methylene)dimalonic acid (ADMDA) (Figure S5) in aqueous solutions. Upon

https://dx.doi.org/10.1021/acsmedchemlett.0c00484
ACS Med. Chem. Lett. 2020, 11, 2491−2496

irradiation of MAO-A/B treated **R1** with a 595 nm LED (20 mW/cm^2), a gradual decrease in the absorbance of ADMDA at 380 nm was detected in each case, proving the photosensitized $^1O_2$ generation (Figures 3b and S6−S7). No detectable decrease was observed in trap absorbance when **R1** was irradiated in the absence of an enzyme (Figures 3b and S8). The $^1O_2$ quantum yields were calculated by using methylene blue (Φ_Δ = 0.52 in PBS buffer)[31] (Figure S9) as a reference and found to be 0.37 and 0.28 for **R1**+MAO-A/B, respectively (Table S1). Different $^1O_2$ yields can be attributed to different cleavage yields of MAO isoforms as evidenced from the higher absorption signal of **R1**+MAO-A. We further demonstrated the $^1O_2$ generation by monitoring the phosphorescence signal of $^1O_2$ at 1270 nm in aqueous solutions. Both **R1**+MAO-A/B gave emission peaks but with a stronger signal in the case of MAO-A, while no sign of $^1O_2$ generation was observed in the case of untreated **R1** (Figure S10), which are all consistent with the trap experiments.

Next, we investigated the *in vitro* PDT effect of **R1** in cancerous MCF-7 (breast cancer, MAO positive)[32,33] and SH-SY5Y (neuroblastoma, high MAO-A activity)[34,35] and normal NIH/3T3[27,28] cells (Table S2). Cells were initially irradiated with a LED light (595 nm, 20 mW/cm^2) for 4 h before cytotoxicity was examined by MTT assay in order to see the performance of **R1** clearly. Cell viabilities decreased gradually in both cancer cells as the drug concentration increases (Figures 4 a and S11); however, the potency of **R1** was found to be substantially higher on SH-SY5Y (IC_{50} = 0.42 μM) cells compared to MCF-7 cells (IC_{50} = 4.0 μM). These results demonstrate that **R1** can be activated by an endogenous MAO enzyme and induce PDT action in SH-SY5Y and MCF-7 cell cultures with a much higher efficiency in MAO-A expressing SH-SY5Y cells. **R1** exhibited substantially lower phototoxicity in noncancerous NIH/3T3 cells (IC_{50} = 6.5 μM) compared to SH-SY5Y cells, when the same drug doses were employed, and the differential activation appeared to be more pronounced at slightly higher concentrations. As shown in Figures 4a and S12, NIH/3T3 cells incubated with 2.5 μM **R1** maintained 70% cell viability, while SH-SY5Y cells showed only 3% viability at the same concentration. Additionally, **R1** showed negligible dark toxicity in both cell types. Although there are numerous factors affecting the efficacy of PDT agents, different photocytotoxicities in three cell lines can be largely attributed to different MAO activities. mRNA expression data imply that the transcript level of MAO-A in SH-SY5Y is 3.74-fold compared to that of MCF-7 (10.1 pTPM/2.7 pTPM).[36−38] Additionally, MAO-B transcript levels are much lower than MAO-A in both cell lines, but still SH-SY5Y has better expression (3-fold).[36−38] These values suggest that total MAO activity in SH-SY5Y cells is higher than MCF-7 cells. This is in line with the **R1** IC_{50} values that were detected in these cells. On the other side, it is a known fact that the MAO activity is very low in NIH-3T3 cells.[27,28] This is also in good correlation with our cytotoxicity results.

Photocytotoxicity of **R1** in SH-SY5Y and NIH-3T3 cells was also tested upon 30 min irradiation to see its performance under shorter irradiation time. IC_{50} value of **R1** increased to 1.90 μM in cancer cells, while no cytotoxicity was observed in normal cells (Figures 4b and S13, Table S2). Thus, **R1** also shows selective phototoxicity upon 30 min irradiation. Moreover, it was shown that the light source did not cause any toxicity during 4 h irradiation (Figure S14), and the phototoxicity index of **R1** was found to be in acceptable limits (Table S2).[39] As a result of *in vitro* cytotoxicity experiments, SH-SY5Y neuroblastoma cells were chosen as a model cell line for detailed imaging studies.

To further support intracellular $^1O_2$ activity, generation of $^1O_2$ was also monitored in SH-SY5Y cells by using cell permeable reactive oxygen species (ROS) sensor 2′,7′-dichlorofluorescein diacetate ($DCFH_2$-DA), which emits green emission upon oxidation. Irradiation of **R1** and $DCFH_2$-DA incubated SH-SY5Y cells gave a strong green emission, which clearly indicates the ROS generation (Figure 5). As $DCFH_2$-DA is not selective toward $^1O_2$, we pretreated a group of SH-SY5Y cells with NaN_3, a known $^1O_2$ quencher,[40]

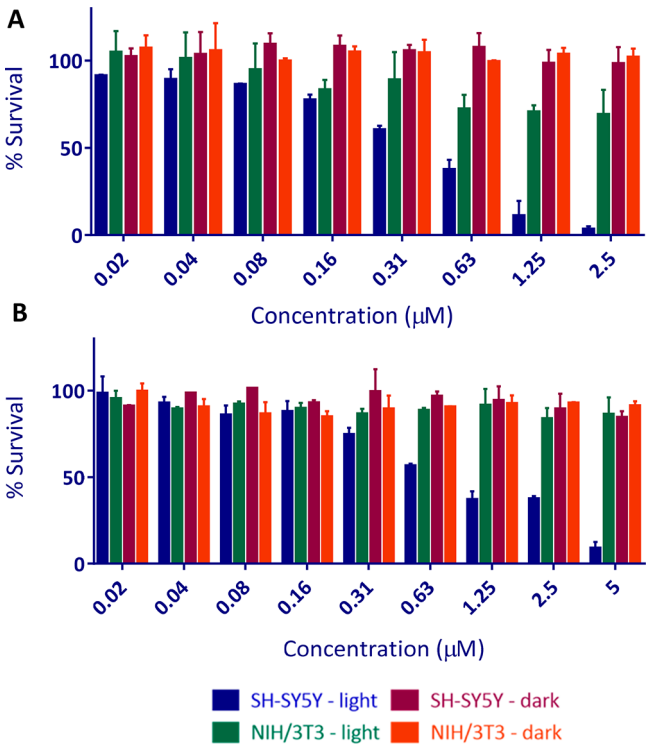

Figure 4. *In vitro* cell viability of SH-SY5Y and NIH/3T3 cells. The cells were incubated with varying concentrations of **R1** and either kept in dark or irradiated for (a) 4 h or (b) 30 min with a 595 nm LED (20 mW/cm^2).

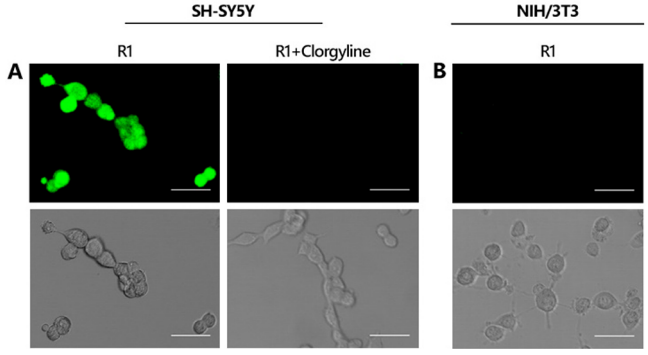

Figure 5. Monitoring ROS production by using sensor $DCFH_2$-DA in (a) SH-SY5Y and (b) NIH/3T3 cells. Cells were incubated with **R1** for 3 h and irradiated with a LED (20 mW/cm^2) for 30 min. For inhibition experiment, SH-SY5Y cells were incubated with clorgyline (0.1 μM) for 30 min in advance. Scale: 50 μm.

https://dx.doi.org/10.1021/acsmedchemlett.0c00484
ACS Med. Chem. Lett. 2020, 11, 2491−2496

in order to show that the generated ROS is actually $^1O_2$. The emission was quenched in NaN_3 treated cells, suggesting **R1** produces $^1O_2$ as a primary cytotoxic agent (Figure S15). In order to prove the activation of **R1** is triggered by MAO-A, ROS imaging was also repeated in the presence of a specific MAO-A inhibitor clorgyline.[41] ROS sensor showed no obvious fluorescence signal in inhibitor treated SH-SY5Y cells as MAO-A activity was significantly diminished (Figure 5). Similarly, very weak fluorescence in normal NIH/3T3 cells is in good agreement with the MTT results. As additional control experiments, a group of SH-SY5Y cells were incubated with **R1** and the sensor but kept under dark and another group of cells were irradiated with a 595 nm LED after incubating ROS sensor only without **R1**. No remarkable fluorescence was detected in both cases as expected (Figure S15).

Photoinduced cell death was further confirmed under confocal microscopy. In this direction, **R1** (2.5 μM) treated SH-SY5Y cells were stained with annexin V-FITC and propidium iodide (PI). Annexin V-FITC selectively binds to phosphatidylserines, which are flipped to the extracellular side of the cell membrane during early apoptosis, and emits green fluorescence. On the other side, red-emitting PI stains the late apoptotic or necrotic cells as it can only permeate through the leaky cell membrane of the dead cells. As shown in Figures 6

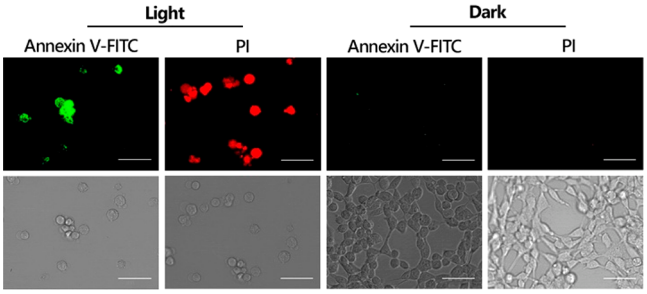

Figure 6. Confocal microscope images of Annexin V-FITC and PI stained SH-SY5Y cells. Cells were incubated with **R1** (2.5 μM) and either kept under dark or irradiated with a 595 nm LED (20 mW/cm^2) for 4 h. Scale: 50 μm.

and S16, both green and red emission were detected after PDT action, clearly indicating the efficient cell death. When SH-SY5Y cells were kept under the dark, no fluorescence was observed, supporting the lack of dark cytotoxicity.

In summary, we have synthesized a MAO-activatable iodinated resorufin derivative (**R1**), which can be obtained only in three steps, and evaluated its $^1O_2$ generation capacity. **R1** showed high $^1O_2$ quantum yields in aqueous solutions in the presence of MAO and was further tested in cell culture studies. Our results showed that **R1** is highly efficient in SH-SY5Y cancer cells with high MAO-A expression, and it can successfully induce differential cytotoxicity between cancer and normal cells. This work introduces a new activatable PS platform, which holds a great promise toward realization of highly effective and cancer cell selective PDT drugs. We believe that heavy atom decorated resorufin cores can be modified with different cage groups to target a variety of cancer cells and more importantly π-extension on the resorufin core may lead to further red-shifted PSs that are suitable for *in vivo* PDT action. Our work along these directions is in progress.

■ ASSOCIATED CONTENT

Supporting Information

The Supporting Information is available free of charge at https://pubs.acs.org/doi/10.1021/acsmedchemlett.0c00484.

Synthetic details, ^1H, ^{13}C NMR, HR-MS spectra, and HPLC chromatogram; details of photophysical characterization, fluorescence spectra, additional photophysical measurements, and a table for photophysical data; singlet oxygen trap experiments and phosphorescence measurements; details of cell culture and imaging experiments, additional cell culture experiments, and a table for cell viability results (PDF)

■ AUTHOR INFORMATION

Corresponding Authors

Gulnihal Ozcan − *Department of Medical Pharmacology, School of Medicine, Koc University, 34450 Istanbul, Turkey*; Email: guozcan@ku.edu.tr

Gorkem Gunbas − *Department of Chemistry, Middle East Technical University (METU), 06800 Ankara, Turkey*; orcid.org/0000-0003-2279-3032; Email: ggunbas@metu.edu.tr

Safacan Kolemen − *Department of Chemistry, Surface Science and Technology Center (KUYTAM), Boron and Advanced Materials Application and Research Center, and TUPRAS Energy Center (KUTEM), Koc University, Sariyer 34450, Istanbul, Turkey*; orcid.org/0000-0003-4162-5587; Email: skolemen@ku.edu.tr

Authors

Toghrul Almammadov − *Department of Chemistry, Koc University, Sariyer 34450, Istanbul, Turkey*; orcid.org/0000-0002-1336-4650

Gizem Atakan − *Department of Chemistry, Middle East Technical University (METU), 06800 Ankara, Turkey*

Ozen Leylek − *Graduate School of Health Sciences, Koc University, 34450 Istanbul, Turkey*; orcid.org/0000-0001-5772-725X

Complete contact information is available at: https://pubs.acs.org/10.1021/acsmedchemlett.0c00484

Author Contributions

The manuscript was written by G.O., G.G., and S.K. T.A., G.A., and O.L. did the experiments. All authors have given approval to the final version of the manuscript.

Funding

Koc University Seed Funding, Middle East Technical University − BAP. The research leading to these results has received funding from the European Research Council (ERC) under the European Union's Horizon 2020 research and innovation program (Grant agreement No. [852614]).

Notes

The authors declare no competing financial interest.

■ ACKNOWLEDGMENTS

The authors are grateful to Işınsu Baylam from KUYTAM-Koc University for the fluorescence quantum yield and singlet oxygen phosphorescence measurements. The authors gratefully acknowledge use of the services and facilities of the Koc University Research Center for Translational Medicine (KUTTAM) funded by the Presidency of Turkey, Presidency

of Strategy and Budget. The content is solely the responsibility of the authors and does not necessarily represent the official views of the Presidency of Strategy and Budget.

■ ABBREVIATIONS

MAO, monoamine oxidase; MAO-A, monoamine oxidase-A; MAO-B, monoamine oxidase-B; PDT, photodynamic therapy; PS, photosensitizer; PBS, phosphate buffer saline; ISC, intersystem crossing; H_2O_2, hydrogen peroxide; DMSO, dimethyl sulfoxide; ADMDA, 2,2′-(anthracene-9,10-diyl)bis-(methylene)dimalonic acid; MTT, 3-(4,5-dimethylthiazolyl-2)-2,5-diphenyltetrazolium bromide; ROS, reactive oxygen species; PI, propidium iodide; $DCFH_2$-DA, 2′,7′-dichlorofluorescein diacetate; HR-MS, high resolution mass spectrometry; OD, optical density; LED, light emitting diode; FITC, fluorescein isothiocyanate; IC50, half maximal inhibitory concentration

■ REFERENCES

(1) Dolmans, D. E.; Fukumura, D.; Jain, R. K. Photodynamic Therapy for Cancer. *Nat. Rev. Cancer* **2003**, *3*, 380−387.
(2) Li, X.; Lee, S.; Yoon, J. Supramolecular Photosensitizers Rejuvenate Photodynamic Therapy. *Chem. Soc. Rev.* **2018**, *47*, 1174−1188.
(3) Beharry, A. A. Next-Generation Photodynamic Therapy: New Probes for Cancer Imaging and Treatment. *Biochemistry* **2018**, *57*, 173−174.
(4) Celli, J. P.; Spring, B. Q.; Rizvi, I.; Evans, C. L.; Samkoe, K. S.; Verma, S.; Pogue, B. W.; Hasan, T. Imaging and Photodynamic Therapy: Mechanisms, Monitoring, and Optimization. *Chem. Rev.* **2010**, *110*, 2795−2838.
(5) Li, X.; Kolemen, S.; Yoon, J.; Akkaya, E. U. Activatable Photosensitizers: Agents for Selective Photodynamic Therapy. *Adv. Funct. Mater.* **2017**, *27*, 1604053.
(6) Macdonald, I. J.; Dougherty, T. J. Basic Principles of Photodynamic Therapy. *J. Porphyrins Phthalocyanines* **2001**, *5*, 105−129.
(7) Majumdar, P.; Nomula, R.; Zhao, J. Activatable Triplet Photosensitizers: Magic Bullets for Targeted Photodynamic Therapy. *J. Mater. Chem. C* **2014**, *2*, 5982−5997.
(8) Bruemmer, K. J.; Crossley, S. W. M.; Chang, C. J. Activity-Based Sensing: A Synthetic Methods Approach for Selective Molecular Imaging and Beyond. *Angew. Chem., Int. Ed.* **2020**, *59*, 13734−13762.
(9) Kolemen, S.; Işık, M.; Kim, G. M.; Kim, D.; Geng, H.; Buyuktemiz, M.; Karatas, T.; Zhang, X.-F.; Dede, Y.; Yoon, J.; Akkaya, E. U. Intracellular Modulation of Excited-State Dynamics in a Chromophore Dyad: Differential Enhancement of Photocytotoxicity Targeting Cancer Cells. *Angew. Chem., Int. Ed.* **2015**, *54*, 5340−5344.
(10) Zeng, Q.; Zhang, R.; Zhang, T.; Xing, D. H_2O_2-Responsive Biodegradable Nanomedicine for Cancer-Selective Dual-Modal Imaging Guided Precise Photodynamic Therapy. *Biomaterials* **2019**, *207*, 39−48.
(11) Tian, J.; Zhou, J.; Shen, Z.; Ding, L.; Yu, J.-S.; Ju, H. A pH-Activatable and Aniline-Substituted Photosensitizer for near-Infrared Cancer Theranostics. *Chem. Sci.* **2015**, *6*, 5969−5977.
(12) Lovell, J. F.; Liu, T. W. B.; Chen, J.; Zheng, G. Activatable Photosensitizers for Imaging and Therapy. *Chem. Rev.* **2010**, *110*, 2839−2857.
(13) Shao, S.; Rajendiran, V.; Lovell, J. F. Metalloporphyrin Nanoparticles: Coordinating Diverse Theranostic Functions. *Coord. Chem. Rev.* **2019**, *379*, 99−120.
(14) Lv, W.; Chi, S.; Feng, W.; Liang, T.; Song, D.; Liu, Z. Development of a Red Absorbing Se-Rhodamine Photosensitizer and Its Application for Bio-Orthogonally Activatable Photodynamic Therapy. *Chem. Commun.* **2019**, *55*, 7037−7040.
(15) Lan, M.; Zhao, S.; Liu, W.; Lee, C. S.; Zhang, W.; Wang, P. Photosensitizers for Photodynamic Therapy. *Adv. Healthcare Mater.* **2019**, *8*, 1900132.
(16) Karaman, O.; Almammadov, T.; Gedik, M. E.; Gunaydin, G.; Kolemen, S.; Gunbas, G. Mitochondria-Targeting Selenophene-Modified BODIPY-Based Photosensitizers for the Treatment of Hypoxic Cancer Cells. *ChemMedChem* **2019**, *14*, 1879−1886.
(17) Xu, F.; Li, H.; Yao, Q.; Ge, H.; Fan, J.; Sun, W.; Wang, J.; Peng, X. Hypoxia-Activated NIR Photosensitizer Anchoring in the Mitochondria for Photodynamic Therapy. *Chem. Sci.* **2019**, *10*, 10586−10594.
(18) Gao, W.; Xing, B.; Tsien, R. Y.; Rao, J. Novel Fluorogenic Substrates for Imaging β-Lactamase Gene Expression. *J. Am. Chem. Soc.* **2003**, *125*, 11146−11147.
(19) Albers, A. E.; Rawls, K. A.; Chang, C. J. Activity-Based Fluorescent Reporters for Monoamine Oxidases in Living Cells. *Chem. Commun.* **2007**, *44*, 4647−4649.
(20) Li, H.; Liu, W.; Zhang, F.; Zhu, X.; Huang, L.; Zhang, H. Highly Selective Fluorescent Probe Based on Hydroxylation of Phenylboronic Acid Pinacol Ester for Detection of Tyrosinase in Cells. *Anal. Chem.* **2018**, *90*, 855−858.
(21) Youdim, M. B. H.; Edmondson, D.; Tipton, K. F. The Therapeutic Potential of Monoamine Oxidase Inhibitors. *Nat. Rev. Neurosci.* **2006**, *7*, 295−309.
(22) Matsumoto, K.; Akao, Y.; Yi, H.; Shamoto-Nagai, M.; Maruyama, W.; Naoi, M. Overexpression of Amyloid Precursor Protein Induces Susceptibility to Oxidative Stress in Human Neuroblastoma SH-SY5Y Cells. *J. Neural Trans.* **2006**, *113*, 125−135.
(23) Liu, F.; Hu, L.; Ma, Y.; Huang, B.; Xiu, Z.; Zhang, P.; Zhou, K.; Tang, X. Increased Expression of Monoamine Oxidase A Is Associated with Epithelial to Mesenchymal Transition and Clinicopathological Features in Non-Small Cell Lung Cancer. *Oncol. Lett.* **2017**, *15*, 3245−3251.
(24) Ugun-Klusek, A.; Theodosi, T. S.; Fitzgerald, J. C.; Burté, F.; Ufer, C.; Boocock, D. J.; Yu-Wai-Man, P.; Bedford, L.; Billett, E. E. Monoamine Oxidase-A Promotes Protective Autophagy in Human SH-SY5Y Neuroblastoma Cells through Bcl-2 Phosphorylation. *Redox Biol.* **2019**, *20*, 167−181.
(25) Lin, Y.-C.; Chang, Y.-T.; Campbell, M.; Lin, T.-P.; Pan, C.-C.; Lee, H.-C.; Shih, J. C.; Chang, P.-C. MAOA-a Novel Decision Maker of Apoptosis and Autophagy in Hormone Refractory Neuroendocrine Prostate Cancer Cells. *Sci. Rep.* **2017**, *7*, 46338.
(26) Huang, J.; Hong, D.; Lang, W.; Liu, J.; Dong, J.; Yuan, C.; Luo, J.; Ge, J.; Zhu, Q. Recent Advances in Reaction-Based Fluorescent Probes for Detecting Monoamine Oxidases in Living Systems. *Analyst* **2019**, *144*, 3703−3709.
(27) Yang, Z.; Li, W.; Chen, H.; Mo, Q.; Li, J.; Zhao, S.; Hou, C.; Qin, J.; Su, G. Inhibitor structure-guided design and synthesis of near-infrared fluorescent probes for monoamine oxidase A (MAO-A) and its application in living cells and in vivo. *Chem. Commun.* **2019**, *55*, 2477−2480.
(28) Li, L.; Zhang, C.-W.; Ge, J.; Qian, L.; Chai, B.-H.; Zhu, Q.; Lee, J.-S.; Lim, K.-L.; Yao, S. Q. A Small-Molecule Probe for Selective Profiling and Imaging of Monoamine Oxidase B Activities in Models of Parkinson's Disease. *Angew. Chem., Int. Ed.* **2015**, *54*, 10821−10825.
(29) McCullagh, J. V.; Daggett, K. A. Synthesis of Triarylmethane and Xanthene Dyes Using Electrophilic Aromatic Substitution Reactions. *J. Chem. Educ.* **2007**, *84*, 1799−1802.
(30) Han, B. H.; Zhou, M.; Vellimana, A. K.; Milner, E.; Kim, D. H.; Greenberg, J. K.; Chu, W.; Mach, R. H.; Zipfel, G. J. Resorufin analogs preferentially bind cerebrovascular amyloid: Potential use as imaging ligands for cerebral amyloid angiopathy. *Mol. Neurodegener.* **2011**, *6*, 86.
(31) Fernandez, J. M.; Bilgin, M. D.; Grossweiner, L. I. Singlet Oxygen Generation by Photodynamic Agents. *J. Photochem. Photobiol., B* **1997**, *37*, 131−140.

https://dx.doi.org/10.1021/acsmedchemlett.0c00484
ACS Med. Chem. Lett. 2020, 11, 2491−2496

(32) Li, X.; Zhang, H.; Xie, Y.; Hu, Y.; Sun, H.; Zhu, Q. Fluorescent Probes for Detecting Monoamine Oxidase Activity and Cell Imaging. *Org. Biomol. Chem.* **2014**, *12*, 2033.
(33) Shen, W.; Long, S.; Yu, S.; Chen, W.; Zhu, Q. Design, Synthesis, and Evaluation of an Activity-Based Probe for Cellular Imaging of Monoamine Oxidases. *Med. Chem. Res.* **2012**, *21*, 3858−3862.
(34) Naoi, M.; Maruyama, W.; Akao, Y.; Yi, H.; Yamaoka, Y. Involvement of Type A Monoamine Oxidase in Neurodegeneration: Regulation of Mitochondrial Signaling Leading to Cell Death or Neuroprotection. *J. Neur. Transm. Suppl.* **2006**, *21*, 67−77.
(35) Fitzgerald, J. C.; Ufer, C.; Girolamo, L. A. D.; Kuhn, H.; Billett, E. E. Monoamine Oxidase-A Modulates Apoptotic Cell Death Induced by Staurosporine in Human Neuroblastoma Cells. *J. Neurochem.* **2007**, *103*, 2189−2199.
(36) Uhlen, M.; Zhang, C.; Lee, S.; Sjöstedt, E.; Fagerberg, L.; Bidkhori, G.; Benfeitas, R.; Arif, M.; Liu, Z.; Edfors, F.; Sanli, K.; von Feilitzen, K.; Oksvold, P.; Lundberg, E.; Hober, S.; Nilsson, P.; Mattsson, J.; Schwenk, J. M.; Brunnström, H.; Glimelius, B.; Sjöblom, T.; Edqvist, P. H.; Djureinovic, D.; Micke, P.; Lindskog, C.; Mardinoglu, A.; Ponten, F. A pathology atlas of the human cancer transcriptome. *Science* **2017**, *357*, No. eaan2507.
(37) The Human Protein Atlas. https://www.proteinatlas.org/ENSG00000189221-MAOA/summary/rna (accessed 2020-11-13).
(38) The Human Protein Atlas. https://www.proteinatlas.org/ENSG00000069535-MAOB/summary/rna (accessed 2020-11-13).
(39) Kim, K.; Park, H.; Lim, K.-M. Phototoxicity: Its Mechanism and Animal Alternative Test Methods. *Toxicol. Res.* **2015**, *31*, 97−104.
(40) Kuimova, M. K.; Yahioglu, G.; Ogilby, P. R. Singlet Oxygen in a Cell: Spatially Dependent Lifetimes and Quenching Rate Constants. *J. Am. Chem. Soc.* **2009**, *131*, 332−340.
(41) Silverman, R. B. Radical Ideas about Monoamine Oxidase. *Acc. Chem. Res.* **1995**, *28*, 335−342.

https://dx.doi.org/10.1021/acsmedchemlett.0c00484
ACS Med. Chem. Lett. 2020, 11, 2491−2496